Research Article

Visible light sensitization of TiO_2/Ag/N nanostructures synthesized by microwave irradiation for oxidative degradation of organic dyes

Guilherme B. Strapasson[1] · Francine R. Scheffer[1] · Suelen W. Cendron[1] · Felipe de C. Silva[1] · Nicole H. Lazzari[1] · Caio Azambuja[1] · Andressa Peyrot[1] · Daniel E. Weibel[1]

Received: 15 November 2019 / Accepted: 26 February 2020 / Published online: 3 March 2020

Abstract
The synthesis of photocatalysts for organic pollutants degradation is a topic of fundamental interest and practical importance, in particular if using green methodologies. In this study, Methyl Orange (MO) and Indigo Carmine (IC) photodegradation on composite TiO_2 nanostructures containing silver or nitrogen was examined. TiO_2 nanotubes (NTs), TiO_2 nanoparticles (NPs) and Ag NPs were prepared by microwave-assisted chemistry (MWAC) using different precursors. The photocatalysts were characterized by XRD, TEM, UV–Vis, BET, XPS and EIS techniques. The degradation rate of MO by the TiO_2 NTs@Ag NPs photocatalyst, under UV–Vis illumination, was about six times higher than that exhibited by the pristine TiO_2 NTs. Additionally, the photodegradation rate of MO on TiO_2 NTs@Ag NPs under visible light ($\lambda \geq 400$ nm) was more than three times higher than pristine TiO_2 NTs irradiated with UV–Vis light. TiO_2 NPs prepared using a water-soluble titanium complex [TALH: Titanium(IV) bis(ammoniumlactato)dihydroxide] as precursor, presents high photodegradation rate for IC and MO under UV–Vis and only visible light irradiation. The presence of nitrogen in the TiO_2 NPs lead to lower band gap values, compared to pristine NTs, which may explain the visible light activity of this photocatalyst. Additionally, Mott–Schottky analysis gave information about the donor density and the absolute position of the flatband potential of the nanostructured TiO_2 thin film electrodes showing a correlation between those parameters and the photocatalytic observed activity. The present work also shows that a green methodology, such as MWAC, coupled to a mild water-soluble precursor, like TALH, may lead to its use in environmental remediation applications with direct utilization of solar light as a sustainable technology.

Keywords Nanoparticles · Nanotubes · TiO_2 · Silver · Visible light · Photocatalysis · Dyes

1 Introduction

During the present century, the preparation of nanoscale materials has allowed the syntheses of a wide diversity of nanostructures, such as nanotubes (NTs), nanoparticles (NPs), nanorods (NRs), nanoplates and Quantum Dots (QDs). In the photocatalytic field, titanium dioxide (TiO_2) is still one of the mostly investigated materials for the photodegradation of pollutants. It competes efficiently with many different non-TiO_2 oxides nanomaterials for the generation of hydrogen (water splitting reaction) [1]. The main reasons to use TiO_2 are: good chemical stability, high catalytic activity, non-toxicity, easy availability and low cost [2, 3]. In photocatalytic studies, the most used commercial powder dispersion of TiO_2 is the well-known

Electronic supplementary material The online version of this article (https://doi.org/10.1007/s42452-020-2343-x) contains supplementary material, which is available to authorized users.

✉ Daniel E. Weibel, danielw@iq.ufrgs.br | [1]Institute of Chemistry, Universidade Federal Do Rio Grande Do Sul, UFRGS, Avenida Bento Gonçalves 9500, Porto Alegre, RS 91501-970, Brazil.

AEROXIDE®TiO_2 P25. This powder finely divided is also recognized as the standard in photocatalysis [4].

Noble metal NPs can also improve the photocatalytic activity of TiO_2 due to their surface plasmon resonance (SPR) effect, allowing visible light activity [5–8]. The collective oscillation of electrons at the surface of metal NPs can be induced by light irradiation which results in the enhancement of the photocatalytic activity. Recently, a series of studies have been carried out on the SPR phenomena. For example, bimetallic Ag–Pt–TiO_2 nanocomposites prepared by the sol–gel method showed higher photocatalytic activity under visible-light irradiation than the monometallic nanocomposite [9]. Silver/silver chloride nanocubes, well-dispersed on TiO_2 nanofibers showed also higher photocatalytic activity by visible light illumination than pure TiO_2 and Ag/TiO_2 nanofibers for the decomposing of organic contaminants [10]. The SPR was also verified with the impregnation of Cu NPs in TiO_2-graphene (P25-GR) nanocomposite fabricated from P25 titania and graphite oxide by hydrothermal method [11]. The nanocomposites showed visible light absorption and increase in the degradation rate of Methylene Blue compared to the P25-GR composite.

The conventional synthesis of TiO_2 and noble metal nanostructures that use hydrothermal or solvothermal synthesis generate important thermal gradients throughout the reaction system leading to non uniform kinetic reactions [12–14]. Those methods also require long reaction times and high temperatures favoring the aggregation of particles and have been recognized more than a decade ago as inefficient and energy-consuming [15]. In this sense, microwave irradiation has shown much promise as an alternative for delivering efficiently energy to a reaction system. The main merits of microwave-assisted chemistry (MWAC) over conventional heating methods include homogeneous heating, fast nucleation processes, good reproducibility, simple control of the reaction parameters, possibility to use non toxic organic solvents and last but not least, it provides a scale-up platform for applications in the industry [15–17]. TiO_2 nanostructures synthesized by MWAC have been reported in the past [18–20] and recently the work was intensified [16, 21–29]. Preparation of P-doped nanostructures of Fe_2O_3–TiO_2 mixed oxides [21], selective oxidation of TiO_2 nanoestructures [22], noble-metal free co-catalysts decorating inorganic–organic hybrid materials [16], controlled morphologies and phases of $BiVO_4$ [27], CdS NRs-carbon NTs for the H_2 production [28] and synthesis of Au/SnS_2 nanoflowers [29] are current examples of the efficient use of MWAC for preparation of several new nanostructures. Titanate NTs, decorated with anatase NPs, have been recently prepared by a microwave assisted hydrothermal reaction in one step [30]. In spite the photocatalysts synthesized were attracting interest from the point of view of the new nanostructures generated, the visible light activity was not clearly observed. The authors used an excitation light from UV light (380 nm) and the used dye, Remazol blue, degraded 49.5% at the end of 60 min of irradiation without the catalyst. In another work, TiO_2 NT array photoelectrodes prepared by anodization process were decorated with Ag–AgBr NPs [24]. The NPs were deposited by microwave reduction strategy. The prepared photocatalysts exhibited better photocatalytic performance in the wide range of solar spectra than the pure TiO_2 NTs. However, the authors used a traditional anodization process as a first step of the syntheses, which cannot be considered a green methodology.

In many typical syntheses of TiO_2 nanostructures the precursors are dissolved in organic solvents. Contact with the atmosphere needs to be avoided together with the presence of water, because they are easy to hydrolyze. For example, TiO_2 nanosheets were fabricated by hydrothermal treatment of a mixed solution of tetrabutyltitanate and hydrofluoric acid [12]. Titanium (IV) isopropoxide, which can be also flammable, is as well a frequently chemical used for the preparation of TiO_2 nanomaterials [25, 31, 32]. If green methodology is pursued for the preparation of new photocatalysts, environmentally green solvents must be used. Over last years, the interest in the synthesis of titania using water-soluble titanium complexes has increased. The use of new water-soluble titanium complexes has allowed the preparation of crystalline nanostructures with controlled hydrolysis reactions and shapes [33–37]. In this sense the use of a stable water-soluble titania precursor, such as titanium(IV) bis(ammoniumlactato) dihydroxide (TALH) represents one interesting and simple alternative for the preparation of TiO_2 nanostructures [33]. TiO_2 porous thick films, which are suitable to work as photoelectrodes in dye-sensitized solar cells were prepared using TALH by the "doctor blade" technique and UV curing [38]. TiO_2 NPs were assembled with TALH to produce films of TiO_2 with low roughness, high refractive index and high transmittance [39].

In the present work, we extend our previous investigations on the synthesis of new photocatalysts [8, 40–43]. The TiO_2 NTs, TiO_2 NPs, and Ag NPs were prepared using a green microwave-assisted method. The NTs or the NPs were impregnated with Ag NPs or Nitrogen respectively to investigate their visible light activities. The results showed that the degradation of prototype dyes occurs by means of photocatalysis under UV–Vis and using only visible irradiation. Finally, to the best of our knowledge, the combination of a water soluble precursor, such as TALH with MWAC to produce TiO_2 NPs with visible light activity, in only one step, has not been reported so far.

2 Materials and methods

2.1 Materials

Titanium(IV) bis(ammoniumlactato)dihydroxide (TALH, 50 wt% in H_2O), aqueous ammonia solution (28.0–30.0% of NH_3), sodium hydroxide, Nafion perfluorinated resin solution (5 wt% in mixture of lower aliphatic alcohols and water) and silver nitrate were purchased from Sigma–Aldrich and used as received. Titanium dioxide NPs powder, AEROXIDE®TiO_2-P25 from EVONIK (a mixture of about 75% anatase and 25% rutile) was received from Degussa Corporation. Ethylene glycol, ETG ≥ 99% (Sigma–Aldrich), Methyl Orange (MO) (100%) and Indigo Carmine (IC) (100%) were obtained from Merck, Brazil. Polyvinylpyrrolidone (PVP, MW 68,400 g mol^{-1}, Synth) was also used as received.

2.2 Microwave-assisted chemical synthesis

Microwave irradiation was carried out mainly in a commercial instrument MARS 6 (CEM Corporation). The temperature during irradiation was continuously monitored by infrared temperature sensors. Two types of TiO_2 nanostructures, NTs and NPs, were prepared from two different precursors TiO_2-P25 and TALH respectively.

In a typical synthesis of TiO_2 NTs a thermal treatment already reported was adapted [44] by using microwave irradiation as excitation source. The preparation started by mixing 0.75 g of the P25 in 50 mL of NaOH 9 mol L^{-1}. The mixture was heated for 2 h at 180 °C (300 W) in a Teflon cup with continuous magnetic stirring. After cooling and pH neutralization with HCl solution (0.1 mol L^{-1}) the precipitate was washed with distilled water, ethanol and dried at ambient temperature. Finally, the products were thermally treated at 400–600 °C for 3 h under ambient atmosphere with a heating rate of 5 °C min^{-1}.

TiO_2 NPs were prepared following a thermal hydrolysis procedure already reported [45], but again in the present work microwave irradiation was used. Typically, 5 mL of a 50 wt% aqueous TALH solution with the addition of 45 mL of 0.1 mol L^{-1} solution of NH_3 was transferred into a 70 mL Teflon cup and irradiated by microwave for 15 min at 160 °C (800 W). Then, the solution was cooled down in air. The resulting TiO_2 NPs were dried in a Petri dish at 50 °C for 3 h. Finally, the NPs were calcinated in air at 400 °C for 4 h with a heating rate of 5 °C min^{-1}.

Silver NPs were prepared adapting the polyol method previously described using ETG as solvent and PVP as stabilizing agent [46]. Typically, PVP (1.95 g), silver nitrate (0.012 mol L^{-1}, 0.025 g) and ETG (25 mL) were mixed and stirred under ultrasound until total PVP dissolution. The solution was then introduced into a homemade Teflon reactor and irradiated at medium power for 15 or 30 s, using a commercial Panasonic Microwave oven (1600 W of maximum power). Then the solution was cooled down, washed twice with acetone (170 mL), and centrifuged at 6000 RPM for 10 min. The precipitated NPs were resuspended in deionized water.

Finally, the effect of visible light sensitization of Ag NPs in the degradation activity of MO was studied impregnating the prepared TiO_2 NTs with the Ag NPs. The TiO_2 NTs (1 g) were dispersed in 20 mL of Ag NPs suspension and stirred for 2 h under atmospheric conditions. The nanostructures were collected by centrifugation, dried at 60 °C overnight and finally thermal treated at 450–600 °C for 1 h with a heating rate of 10 °C min^{-1}.

2.3 Characterization

The optical properties of the TiO_2 nanostructures were measured using a double-beam CARY 5000 spectrophotometer (Varian) in the wavelength range of 200–800 nm. The bandgap values of samples were determined by UV–Vis measurements with an integrated sphere. The Kubelka–Munk model was used to determine the bandgap assuming that the sample scattering coefficient was constant for the UV–Vis wavelength range [47]. The phase identification of the nanostructures was conducted with X-ray diffraction using a Siemens Goniometer D500 equipped with Cu Kα radiation at 40 kV and 20 mA. The data were collected for scattering angles (2θ) ranging from 20° to 80° with a step size of 0.05°. The results were analyzed using the Crystallographica Search-Match (CSM) software. The nanostructures were also characterized by transmission electron microscope (TEM) JEOL JEM 1200 ExII system (Microscopy Center, UFRGS) and using a transmission electron microscope with a field emission gun (FEG-TEM/STEM: JEM 2100F URP) at the Brazilian Nanotechnology National Laboratory (LNNano), Campinas, SP, Brazil.

TiO_2 thin films for Mott–Schottky measurements were prepared using from 5 to 10 mg mL^{-1} of titanium dioxide precursors in Nafion solution. The films were prepared by casting 500 µL of the precursor mixtures on cleaned Fluorine doped Tin Oxide (FTO) glass substrates. After each coating, the samples were kept at 353 K overnight in air atmosphere, for solvent evaporation. Mott–Schottky analysis was performed at a frequency of 1 kHz with 10 mV of amplitude, with various potentials applied to a standard three-electrode cell on an Autolab potentiostat PGSTAT30. The cell employed Na_2SO_4 0.5 mol L^{-1} as the electrolyte solution, a platinum foil as the counter electrode, a saturated calomel electrode as the reference electrode and

FTO/TiO_2 electrodes, with 1 cm^2 exposed area, as working electrodes.

X-ray photoelectron spectroscopy (XPS) spectra measurements were carried out using a conventional electron spectrometer (Omicron Gmbh, Germany) equipped with a high performance hemispherical energy analyzer and a seven-channeltron detector. Al Kα radiation was used as the excitation source. Surveys spectra were recorded with pass energy of 50 eV, whereas selected atomic signals were acquired with 10 or 20 eV of pass energy depending on the intensity signal measured. In the spectra, the position of the C–C/C–H was specified, and other peaks of different carbon environments were fixed relative to this peak, set at 285.0 eV. The deconvolution of the selected atomic regions was carried out using the Casa XPS software package. The XPS signals were analyzed and peak-fitted after the subtraction of a Shirley background using Gaussian-Lorenzian peak shapes.

The specific surface area and pore size distribution of the TiO_2 nanostructures were calculated from the adsorption/desorption isotherms of N_2 at 77 K by multi-point Brunauer–Emmett–Teller (BET) and Barrett–Joyner–Halenda (BJH) method using a Micromeritics Tristar II 3020 V1.01 instrument.

2.4 Photocatalytic measurements

The photodegradation experiments were carried out using aqueous solutions of MO or IC in a quartz photochemical reactor. An unfiltered or filtered light from a high pressure Xe/Hg lamp of 350 W (Sciencetech Inc.) was used. A Long Wave Pass Filter, 25.4 mm, 400 ± 5 nm cut-on (410–1200 nm) from Newport Corporation was used when only visible light was allowed to enter the reactor. Solutions of 35 mL of MO (12 ppm) or IC (35 ppm) were irradiated at selected time periods and the changes in concentrations of the dyes were monitored regularly by measuring the absorbance at the correspondent wavelength (465 nm and 610 nm for MO and IC respectively).

3 Results and discussion

3.1 Pristine and Ag loaded TiO_2 nanotubes

The XRD pattern of prepared TiO_2 NTs by MWAC and thermal treated at 400 °C is shown in the Fig. 1. Diffractions peaks that are assigned to anataseTiO_2 are clearly observed in the calcinated material. The peaks at 2θ values = 25.2°, 37.8°, 48°, 54.5°, 62.6°, 75° and 82° can be attributed to the anatase phase (JCPDF 87-597) and also agree with previous reported data [44].

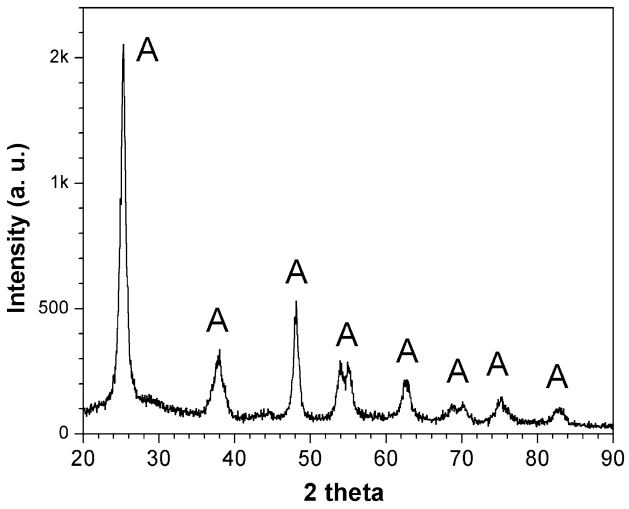

Fig. 1 XRD pattern of the prepared TiO_2 NTs by microwave irradiation at 180 °C and thermal treated at 400 °C. *A* Anatase

The morphologies of the TiO_2 NTs were analyzed by TEM and the results are presented in Fig. 2. The TEM results show well-shaped and randomly oriented NTs with open ends under the present MWAC conditions. The TiO_2 NTs have approximate outer diameters of 8.5 nm, inner diameters of about 3.7 nm and micrometer long. The wall thickness was on average lower than 2.5 nm. The optical properties of the TiO_2 NTs were investigated by the UV–Vis absorption spectra. The measured band gap absorption was 3.47 eV, being slightly higher than the accepted 3.2 eV for the intrinsic band gap absorption of pure anatase (see Fig. S1 in Supporting Information, SI, for more details). The discussion on the band gap measured for the several prepared photocatalysts will be discussed in the photocatalytic activity section.

Silver NPs were prepared using PVP as stabilizing specie. Figure 3 shows the results of the analyses carried out to characterize the prepared Ag NPs. The UV–Vis spectra of the Ag NPs stabilized with PVP can be seen in Fig. 3a. Ag/PVP NPs show a stronger photoabsorption in the visible region at about 400–410 nm mainly due to the surface plasmonic resonance (SPR) effect of the Ag NPs [48]. Figure 3a also shows that there is a shift to longer wavelengths in the UV maximum absorption. Because the dielectric constant of the medium and the stabilizing specie (PVP) were the same and only the time of irradiation changed, the shape and position of the plasmon absorption in the SPR maximum has to be related to changes in particle size of prepared Ag NPs [49]. The change in the maximum from 398 nm (15 s) to longer wavelengths, 409 nm (30 s), is due to changes in the NPs size. Figure 3b shows that the Ag NPs formed with 15 s of microwave irradiation has a main bimodal

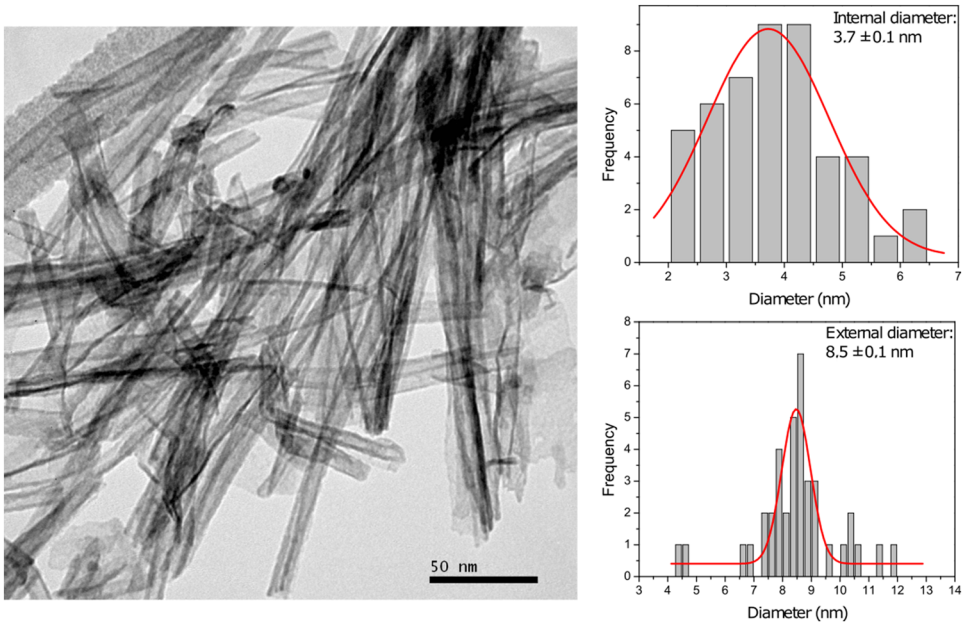

Fig. 2 TEM image of TiO_2 NTs prepared by microwave irradiation at 180 °C and calcinated at 400 °C (left). The external and internal NTs diameters were calculated and they are also shown (right)

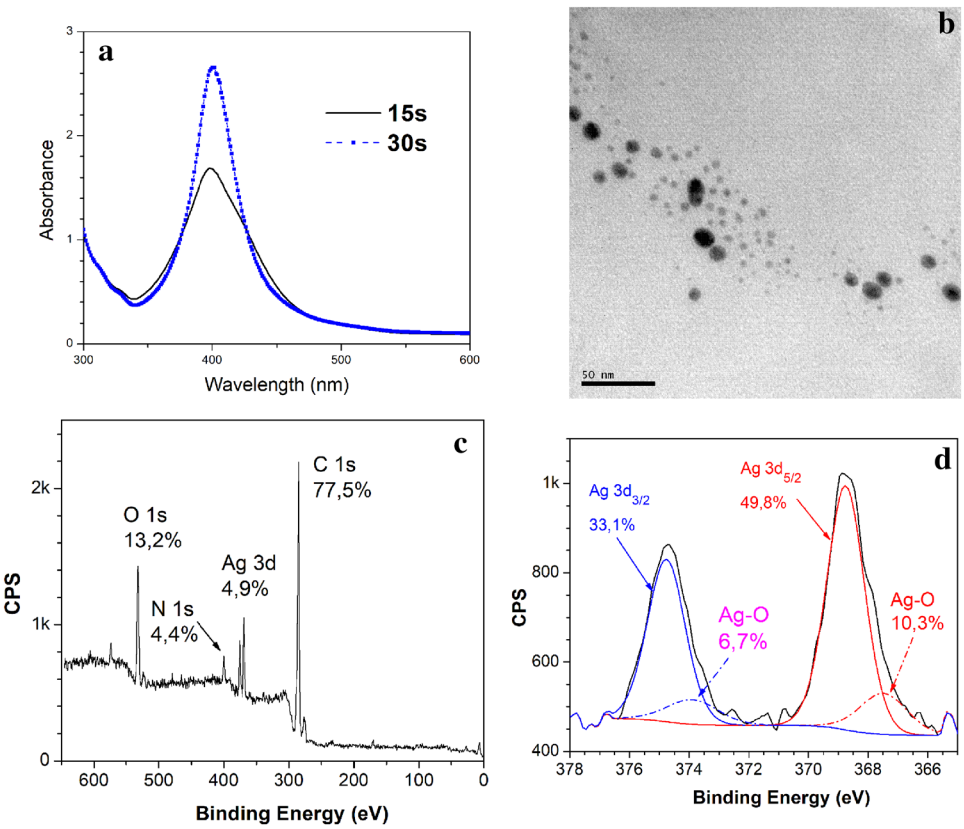

Fig. 3 Characterization of the prepared Ag NPs by MWAC adapting the polyol method: **a** UV–Vis absorption spectra at two different microwave irradiation times, **b** TEM analyses, **c** XPS survey spectrum and **d** XPS signal analyze of the Ag 3*d* envelope

distribution with NPs diameter distributions below 1 and 2 nm (0.75 ± 0.05 and 1.8 ± 0.1 respectively). When the irradiation time increased to 30 s, a multimodal size distribution of Ag NPs was obtained with NPs sizes ranged from about 1–12 nm (see Fig. S2 in SI).

XPS spectroscopy was also used to confirm the presence of silver and its oxidation state. The results are shown in Fig. 3c, d. Figure 3c shows clearly the presence of Ag 3*d* signals together with the N 1*s*, corresponding to the PVP. The Ag $3d_{5/2}$ and Ag $3d_{3/2}$ peaks appear at 368.8 eV

and 374.8 eV, respectively, with the splitting of the 3*d* doublet of 6.0 eV, supporting what should be expected [50]. Additionally, Fig. 3d evidences a partial oxidation of the Ag NPs in an amount lower than about 10% that shows the presence of Ag_2O or AgO 3*d* signals in the spectrum. Due to the similarity in the binding energy between Ag_2O and AgO and the maximum resolution that it should be expected in the apparatus used here (~ 1 eV), it is difficult to differentiate between Ag_2O and AgO.

Finally, the TiO_2 NTs were impregnated with the prepared Ag NPs. Figure 4 shows the XRD pattern of the TiO_2 NTs loaded with the silver NPs after thermal treatment carried out at 600 °C. The presence of Ag can be confirmed with the peaks at 2θ = 38.1°, 44.2° and 58° corresponding to the planes (111), (200) and (103), respectively (JCPDF 1-1164). The other peaks marked with the letter A in Fig. 4 refer to the peaks attributed to the anatase phase (see also Fig. 1). Additional signals at 24.5°, 29.8°, 32.8° and ~ 67° appeared in Fig. 4. It was previously observed that TiO_2 NTs thermal treated at 600 °C or higher temperature exhibited new DRX signals superimposed onto the pattern of typical anatase phase [51]. These new peaks could be assigned to the $Na_2Ti_6O_{13}$ or $Na_2Ti_3O_7$ compounds (peaks marked with * in Fig. 4), originated from the presence of NaOH in the synthesis of the TiO_2 NTs. Ferreira et al. have proposed a general formula after washing the TiO_2 NTs in acid medium as $Na_{2-x}H_xTi_3O_7{\cdot}nH_2O$, $0 \le x \le 2$, where the Na^+ was exchanged by H^+. When the temperature increased to 600 °C and over they observed that the final products of thermal decomposition were $Na_2Ti_6O_{13}$ or $Na_2Ti_3O_7$.

The optical properties of the Ag NPs loaded TiO_2 NTs were investigated also by the UV–Vis absorption spectra. The measured absorption spectra of these samples showed that the band gap absorption was 3.5 eV very close to pristine TiO_2 NTs. It was previously observed that for photocatalysts loaded with low content of silver, the band gap is similar to pristine TiO_2. However, when the amount of silver was increased, a lower values of band gaps were measured [49]. The Fig. 3d shows that the amount of silver on the surface region quantified by XPS is below 5%. In the present study, the Ag NPs have diameters smaller than 2 nm before the impregnation process, but after the thermal treatment at 600 °C partial dissolution and reduction of Ag^+ can proceed [52]. In the work carried out by Amarjargal et al., TiO_2 microrods were prepared by a reflux method followed by heat treatment. Under their experimental conditions, reduction of Ag^+ to Ag^0 was observed at temperatures over 500 °C. The authors assumed that total reduction of silver ions due to the high redox potential of Ag^+ and the low electronegativy of the TiO_2. In the present work the wall thickness of the TiO_2 NTs was about 2.5 nm. It may allow diffusion of the silver ions to the surface through TiO_2 NT walls without reach a complete reduction of silver ions.

The impregnation of the TiO_2 NTs with Ag NPs led to changes in the specific surface area and pore dimensions measured by BET and BJH methods. Compared to pristine TiO_2 NTs, the specific surface area and the pore volume measured after Ag NPs impregnation decreased 22 and 26% respectively (see Table 1). However, the pore size decreased less than 5% with the impregnation of the Ag NPs. Similar results were already observed in the past and they were interpreted as a blocking effect of the TiO_2 capillaries by the silver clusters [49, 53]. Those effects were also observed for commercial TiO_2-P25 NPs [49, 54]. Even so, the presence of Ag NPs is more beneficial for photocatalytic reactions as they improve the interfacial charge transfer between the organic pollutant and TiO-$_2$ NTs.

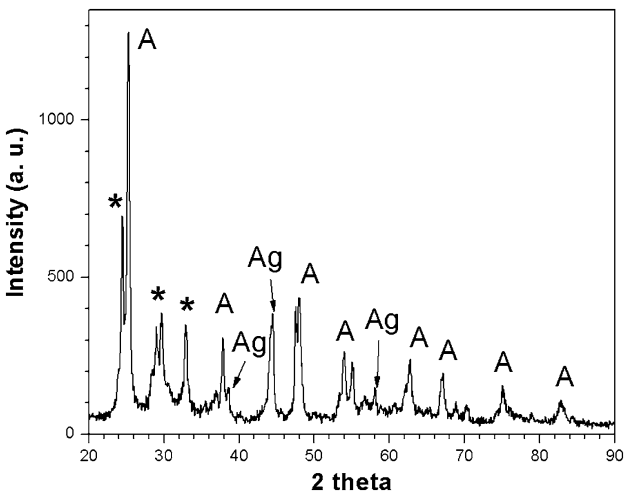

Fig. 4 XRD pattern of the prepared TiO_2 NTs by microwave irradiation at 180 °C and impregnated with Ag NPs, thermal treated at 600 °C for 3 h. *A* Anatase. * $Na_2Ti_6O_{13}$ or $Na_2Ti_3O_7$

3.2 TiO_2 nanoparticles using TALH as precursor

TiO_2 NPs using an environmentally green solvent were prepared using TALH, a stable water-soluble titania precursor, which represents an interesting and simple alternative for the preparation of TiO_2 NPs. Figure 5 shows the XRD pattern of the prepared TiO_2 NPs by MWAC before and after thermal treatment at 400 °C. Diffractions peaks typical

Table 1 Structural characteristics of the photocatalysts: TiO_2 NTs and TiO_2 NTs@AgNPs

Sample	Pore dimension		
	S_{BET} ($m^2\ g^{-1}$)	Volume ($cm^3\ g^{-1}$)	Size (nm)
TiO_2 NTs	234.0	0.669	12.9
TiO_2 NTs@Ag NPs	181.4	0.494	12.3

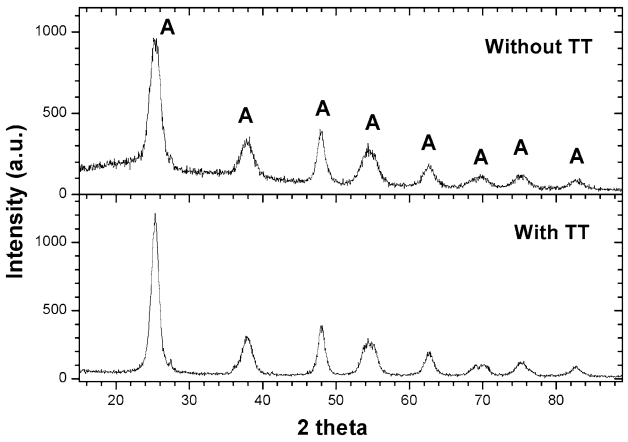

Fig. 5 XRD pattern of the prepared TiO_2 NPs by microwave irradiation from a stable water-soluble titania precursor (TALH) before and after thermal treatment at 400 °C. *TT* Thermal treatment

from anatase TiO_2 (JCPDF 87-597) are clearly observed in the material before and after calcination. TiO_2 NPs were formed with a high degree of crystallinity before calcination. The results showed that the present synthesis of TiO_2 NPs does not need a further thermal treatment for its use as a photocatalysts, because the prepared NPs presented high crystallinity and 100% of the most active TiO_2 phase (anatase) just after the MWAC process.

Figure 6a, b present a typical TEM image of the prepared TiO_2 NPs showing their main size distribution centered at about (5 ± 1) nm. The optical properties of the TiO_2 NPs were also measured and a band gap of 3.1 eV, slightly lower than a typical TiO_2 anatase, was obtained. Because TALH is an ammonium lactatodihydroxide titanium complex and the synthesis was carried out with the addition of NH_3, some degree of nitrogen doping or impregnation may be expected after microwave irradiation and calcination. By XRD analysis (Fig. 5) no presence of nitrogen in the structure was detected probably because its concentration was below the detection limit of the equipment. To confirm the existence of nitrogen in the TiO_2 NPs, XPS measurements were carried out and the results are shown in the Fig. 6c. The survey XPS spectrum shows that the O/Ti ratio is ~ 2.2 very close to the theoretical ratio of 2. In spite the survey spectrum showed very week N 1*s* signal intensity, the inset of Fig. 6c demonstrated the presence of nitrogen in the surface region. This result together with the low band gap of 3.1 eV measured may indicate a small degree of nitrogen doping during the TiO_2 NPs synthesis.

3.3 Photocatalytic activity

The dependence of the degradation rate of MO, used as one prototype dye to test the photodegradation activity, on the concentration of pristine TiO_2 NTs was first

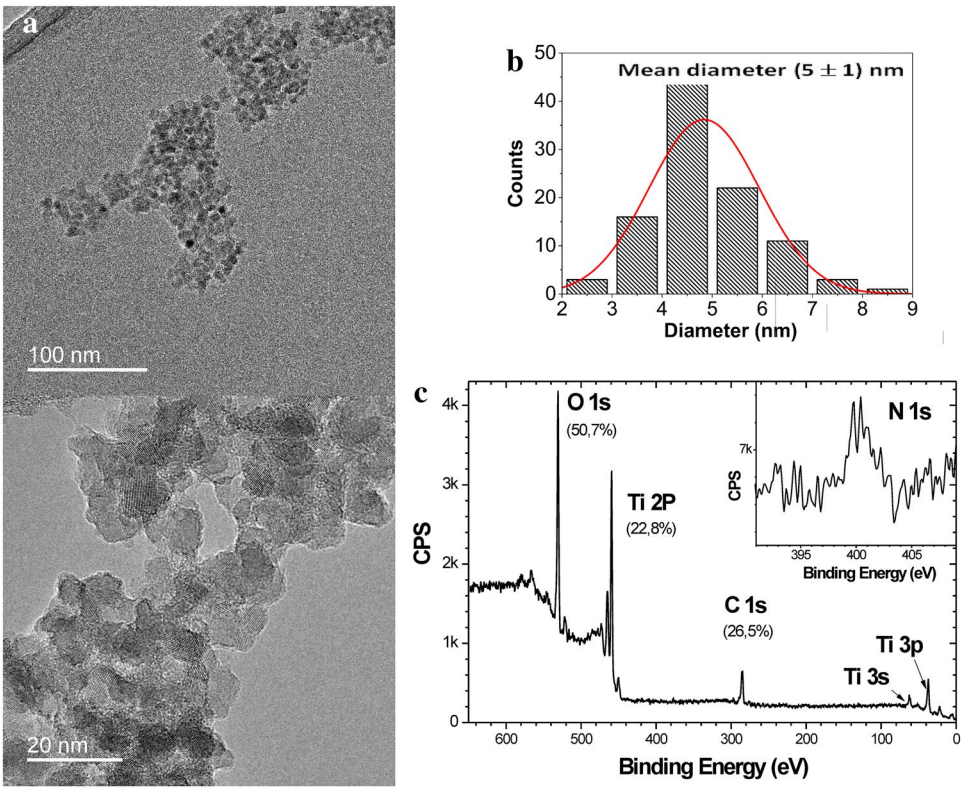

Fig. 6 **a** TEM image of TiO_2 NPs prepared by microwave irradiation from a stable water-soluble titania precursor (TALH) after thermal treatment (TT) at 400 °C in air for 4 h. **b** Average size calculation of the TiO_2 NPs diameter. **c** Survey XPS spectrum of the prepared TiO_2 NPs after TT

determined over the range 1–5 mg mL^{-1} (see Fig. S3 in SI). As expected, Fig. S3 showed that the degradation rate increased, with the increasing concentration of TiO_2 NTs approaching to a maximum value of about 2.5 mg mL^{-1}. Concentrations higher than about 2.5–2.7 mg mL^{-1} led to a decrease in the MO degradation rate. Two well known factors are responsible for those results: aggregation of the TiO_2 NTs at high concentrations, which decreases the number of the surface active sites and light scattering effects of the TiO_2 NTs when the concentration increases. As a consequence of the Fig S3 results, the concentration used for the present degradation study for the TiO_2 NTs and TiO_2 NTs@Ag NPs photocatalysts was 2.5 mg mL^{-1}.

In photocatalysis the reaction is initiated when a photoelectron is promoted from the filled valence band of a semiconductor photocatalyst to the empty conduction band (CB) as a result of the photon absorption. The process leads to a highly reactive hole in the valence band (VB) and an electron in the CB that is trapped by surface adsorbed O_2 generating several reactive oxidative species. The final $HO^{\cdot}$ radicals formed on the irradiated semiconductor surface are extremely powerful oxidizing agents and they are the basis of the Advanced Oxidation Processes (AOPs) that constitute a promising technology for the treatment of wastewaters containing organic compounds [55, 56]. The Langmuir–Hinshelwood mechanism can be used to express the rate of the heterogeneous photocatalytic degradation of a dye according to the following mathematical equation [57]:

$$r = -\frac{dC}{dt} = \frac{kK_{ad}C}{1 + K_{ad}C} \quad (1)$$

where r represents the initial rate of photooxidation, C is the dye concentration that depends on time t, k is the reaction rate constant, and K_{ad} is the adsorption coefficient of the dye on the photocatalyst. Pseudo-first-order reaction conditions can be applied when the dye concentration is low enough and the product $K_{ad}C$ is very small compared with 1, leading to the integration of Eq. (1) led to Eq. (2):

$$\ln \frac{C_0}{C} = kK_{ad}C = k_{app}t \quad (2)$$

where $k_{app} = kK_{ad}$ is the apparent pseudo-first-order reaction rate constant and C_0 is the initial concentration of the dye.

Figure 7 shows the linear relationship of the natural logarithm of the ratio between the initial concentration of the dye and the concentration after photocatalytic degradation ($\ln(C_0/C_t)$) versus the corresponding irradiation time for the MO degradation. It can be observed in Fig. 7 the results achieved under UV–Vis irradiation and with only visible illumination (λ ≥ 400 nm) for pristine TiO_2 NTs and Ag NPs loaded TiO_2 NTs. Those results indicate that the photocatalytic degradation of MO can be described by the first-order kinetic model for both photocatalysts (Eq. 2). The value of k_{app} obtained from the slopes of the linear curves show that under UV–Vis illumination the TiO_2 NTs@Ag NPs photocatalyst is about six-folds higher than pristine TiO_2 NTs for the MO photodegradation. Irradiation of the pristine TiO_2 NTs with only visible light (λ ≥ 400 nm) almost did not produce any MO degradation. On the contrary when TiO_2 NTs@Ag NPs photocatalyst was illuminated with visible light the MO photodegradation process is evident. The k_{app} calculated is more than three times higher than pristine TiO_2 NTs illuminated with UV–visible light. The above results demonstrated that the SPR effect is efficient for the photocatalytic decomposition of MO under UV–Vis and also with only visible light exposure.

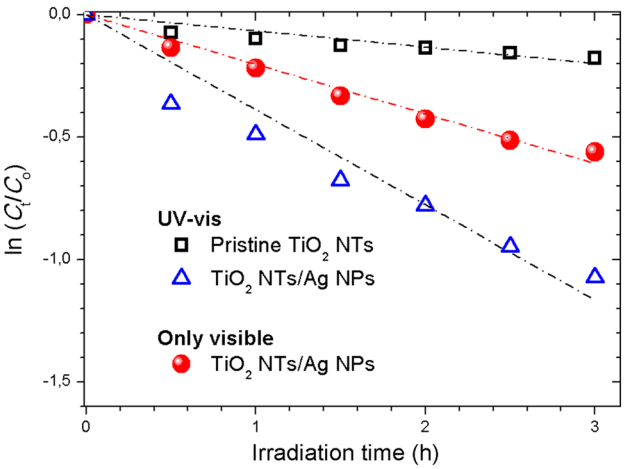

Fig. 7 Kinetics of Methyl Orange photocatalytic degradation on pure TiO_2 NTs and loaded with Ag NPs under UV–Vis and visible light illumination (λ ≥ 400 nm). MO concentration = 12 ppm

The photocatalytic properties of TiO_2 NPs prepared using TALH as precursor were tested for the photodegradation of Indigo Carmine (IC). Figure 8 shows the results obtained when a solution of 35 ppm of IC was mixed with 1 mg mL^{-1} of the prepared TiO_2 NPs and illuminated. IC has a low photodegradation rate under UV–Vis irradiation, but no degradation was detected under only visible illumination (see Fig. 8). The k_{app} calculated for IC irradiated with UV–Vis light showed that the presence of TiO_2 NPs in the solution increased the photodegradation rate nearly 14 times. Irradiation with only visible light illumination of the IC solutions in the presence of the TiO_2 NPs prepared using TALH as precursor showed that the photodegradation is about twice times more efficiently than the irradiation of IC solution with UV–Vis light or IC solution with UV–Vis light in the presence of commercial P25 TiO_2. A comparison with commercial P25 TiO_2 NPs is also included in Fig. 8 for only visible light irradiation. As can

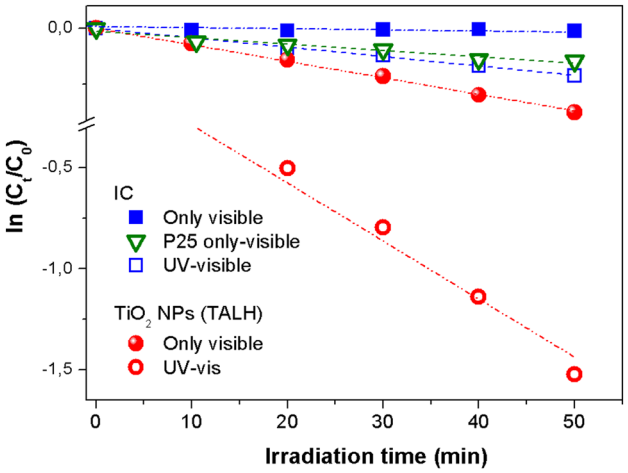

Fig. 8 Kinetics of the photodegradation of Indigo Carmine solutions with and without the addition of TiO_2 NPs prepared using TALH as precursor. The results under UV–Vis and visible light irradiation ($\lambda \geq 400$ nm) are presented together. IC concentration = 35 ppm. NPs concentrations = 1 mg mL^{-1}. A comparison with the commercial P25 TiO_2 is also included

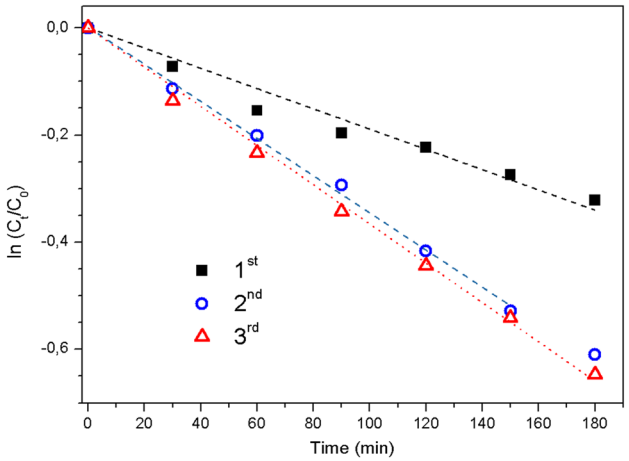

Fig. 9 UV–Vis photocatalytic degradation cycling curves for the photodegradation of Methyl Orange, MO, solutions in the presence of TiO_2 NPs prepared using TALH as precursor. MO concentration = 12 ppm. NPs concentrations = 1 mg mL^{-1}

be seen in the figure no increase in the IC degradation rate was observed under the presence of P25 TiO_2 NPs. This result shows the very low absorption coefficient of P25 for photons at wavelength longer than 400 nm. The presence of nitrogen in the surface region of the TiO_2 NPs prepared by MWAC (see Fig. 6) and its lower band gap measured may explain their visible light activity.

The stability of the TiO_2 NPs photocatalyst prepared using TALH as precursor was evaluated by cycling experiments and the results are shown in Fig. 9 for the degradation of MO. After each cycle the catalyst was collected by centrifugation and washed with distilled water. Then the washed catalyst was used again with a fresh MO solution for the degradation of the dye. The data indicates that the catalyst was reusable at least for three runs. After the first cycle the degradation rate remained constant for more two repeated cycling runs, showing its outstanding stability.

Finally, to understand better the band structures of the TiO_2 samples and the photocatalytic results, Mott–Schottky analysis was carried out. Electrochemical impedance spectroscopy allows obtaining information about the donor density (N_D) and the absolute position of the flatband potentials (V_{fb}) of the nanostructured TiO_2 thin film electrodes [58–62]. Figure 10 shows that all samples have a quasi-linear behavior with positive slopes, indicating the characteristics of n-type semiconductors [58]. The V_{fb} and the N_D of the TiO_2 thin films were obtained from Mott–Schottky plots (taken in the dark, see Fig. 10) and using the following equation :

$$\frac{1}{C^2} = \frac{2}{\varepsilon_{TiO_2}\,\varepsilon_0\,e\,N_D}\left(V - V_{fb} - \frac{kT}{e}\right) \quad (3)$$

where ε_{TiO_2} is the permittivity of the semiconductor electrode, ε_0 the permittivity of free space, e the elementary charge, V the applied potential, k the Boltzmann's Constant, T the temperature during the experiments and C the space charge capacitance. By using Eq. (3), a plot of ($1/C^2$) vs V would lead to a straight line, intersecting the potential axis at V_{fb}. By the slope of the line the respective N_D can then be calculated.

For n-type semiconductors it is possible to assume that the difference between the V_{fb} and the energy level of the conduction band (CB) minimum is negligible [63, 64]. By this way the valence band (VB) level can be calculated if the band gap energy is known from optical measurements. A summary of the calculations is presented in Table S1 (SI). Films that exhibited a more negative V_{fb} were found to have higher N_D values and also showed higher photocatalytic activities compared to TiO_2 P25. The donor density of the TiO_2 NTs@Ag NPs and TiO_2 NPs (TALH) improved about 4.9 and 4.3 respectively in relation to TiO_2 P25 (see Fig. 10 and Table S1). It is possible that the enhancement in the N_D is originated from the incorporation of Silver and Nitrogen respectively, which modified strongly the CB level of those photocatalysts (see Table S1 in SI). This effect is also observed when the photocatalytic activity is compared between pristine TiO_2 NTs and TiO_2 NTs@Ag NPs. Figure 10a shows a more negative V_{fb} for the TiO_2 NTs@Ag NPs photocatalyst with and approximately 1.5 improvement in the donor density measured in relation to pure TiO_2 NTs (see Table S1 in SI). Taken into account that the specific surface area of the TiO_2 NTs@Ag NPs photocatalyst

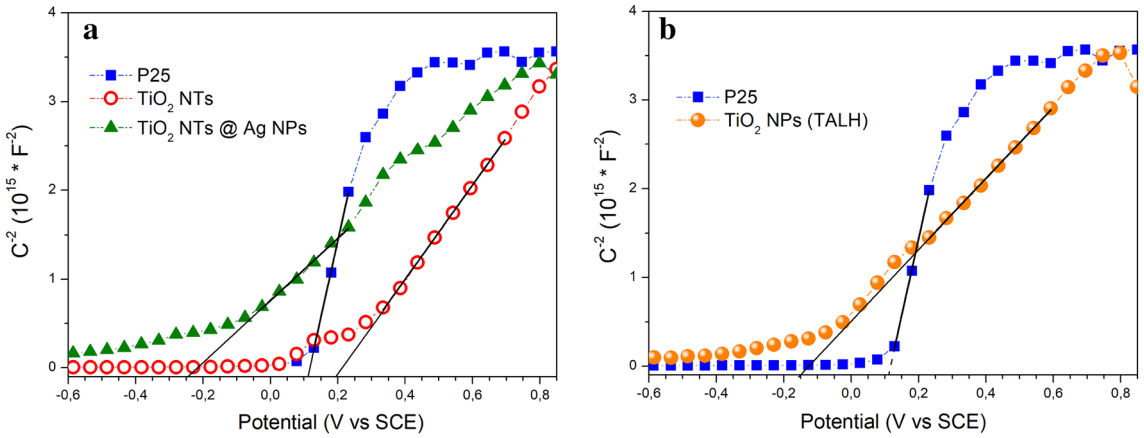

Fig. 10 Dependence of the capacitance on the voltage for the various TiO_2 NTs and NPs prepared films and plotted in conventional Mott–Schottky form. **a** Pristine TiO_2 NTs and loaded with Ag NPs. **b** TiO_2 NPs prepared using TALH as precursor. The plots were recorded at 1 kHz. For the bias voltage polarity used, a positive slope indicates n-type behavior. Data on films prepared using commercial TiO_2 P25 powder are shown for comparison

decreased only 22% in relation to TiO_2 NTs, the about six-folds more efficiency in the MO photodegradation under UV–Vis illumination of the silver impregnated NTs (see Fig. 7) can be assigned to the intrinsic electronic properties of this photocatalyst.

4 Conclusions

The present study exemplifies that the microwave-assisted synthesis methodology is an effective and green strategy to prepare nanostructures, such as nanotubes and nanoparticles. The prepared photocatalysts showed excellent photodegradation properties of aqueous solutions of the two tested prototypes dyes. The results demonstrated that the impregnation of TiO_2 NTs with Ag NPs led to a photocatalyst with more than six times higher activity than pristine TiO_2 NTs. Additionally, the prepared TiO_2 NTs@Ag NPs photocatalysts were active under only visible light irradiation with a photodegradation rate more than three times higher than pristine TiO_2 NTs irradiated with UV–Vis light. These results illustrate the importance of the Ag NPs SPR effect for the induction of photodegradation processes with only visible light irradiation. TiO_2 NPs synthesized by MWAC with a main size distribution about 5 nm were prepared using a different water titania precursor (TALH) and the addition of NH_3. The TiO_2 NPs showed high activity for the photodegradation of IC solutions under UV–Vis and also under only visible illumination. The presence of nitrogen in the TiO_2 NPs and the lower band gap measured may explain the visible light activity of this photocatalyst. The reusability of this photocatalyst was tested for the degradation of the MO dye showing excellent properties at least for three cycles. Mott–Schottky measurements showed that the photocatalytic activity increases with increasing donor density and increasing negative shift of the flatband potential.

The present work also suggests that the use of microwave radiation as a mild and green method coupled to a water soluble precursor, such as TALH may lead to its use in environmental remediation applications with direct utilization of solar light as a sustainable technology.

Acknowledgements This work was mainly supported by the CNPq (Conselho Nacional de Desenvolvimento Científico e Tecnológico), Process No. 402360/2016-8. We thank also the support of CAPES (Coordenação de Aperfeiçoamento de Pessoal de Nível Superior), Brazil, the Microscopy Center-UFRG, CNANO (Centro de Nanociência e Nanotecnologia)-UFRGS. Research supported by LNNano - Brazilian Nanotechnology National Laboratory, CNPEM/MCTIC. S.U.W and G. B. S. acknowledge receipt of CAPES and CNPq fellowships respectively for financial support.

Compliance with ethical standards

Conflict of interest On behalf of all authors, the corresponding author states that there is no conflict of interest.

References

1. Singh R, Dutta S (2018) A review on H_2 production through photocatalytic reactions using TiO_2/TiO_2-assisted catalysts. Fuel 220:607–620
2. Fujishima A, Zhang X, Tryk DA (2008) TiO_2 photocatalysis and related surface phenomena. Surf Sci Rep 63(12):515–582
3. Henderson MA (2011) A surface science perspective on TiO_2 photocatalysis. Surf Sci Rep 66(6–7):185–297
4. Mills A, Lee S-K (2002) A web-based overview of semiconductor photochemistry-based current commercial applications. J Photochem Photobiol A 152(1):233–247

5. Chen XQ, Liu DD, Wu ZS, Cravotto G, Wu ZL, Ye BC (2018) Microwave-assisted rapid synthesis of Ag-beta-cyclodextrin/TiO_2/AC with exposed 001 facets for highly efficient naphthalene degradation under visible tight. Catal Commun 104:96–100
6. Awazu K, Fujimaki M, Rockstuhl C, Tominaga J, Murakami H, Ohki Y, Yoshida N, Watanabe T (2008) A plasmonic photocatalyst consisting of sliver nanoparticles embedded in titanium dioxide. J Am Chem Soc 130:1676–1680
7. Rao VN, Reddy NL, Kumari MM, Cheralathan KK, Ravi P, Sathish M, Neppolian B, Reddy KR, Shetti NP, Prathap P, Aminabhavi TM, Shankar MV (2019) Sustainable hydrogen production for the greener environment by quantum dots-based efficient photocatalysts: a review. J Environ Manag 248:109246
8. Fornari AMD, Araujo MBd, Duarte CB, Machado G, Teixeira SR, Weibel DE (2016) Photocatalytic reforming of Aqueous Formaldehyde with Hydrogen Generation over TiO_2 nanotubes Loaded with Pt or Au nanoparticles. Int J Hydrog Energy 41:11599–11607
9. Zielinska-Jureka A, Wei Z, Wysocka I, Szweda P, Kowalska E (2015) The effect of nanoparticles size on photocatalytic and antimicrobial properties of Ag–Pt/TiO_2 photocatalysts. Appl Surf Sci 353:317–325
10. Tian W, Wu H, Su C, Huang Y, Zhao W, Yang X (2018) Heterostructure based on silver/silver chloride nanocubes loaded titanium dioxide nanofibers: a high-efficient and recyclable visible light-responsive photocatalyst. J Photochem Photobiol A 350:122–129
11. Yang YH, Huang WH (2018) Design of copper and titanium dioxide nanoparticles doped with reduced graphene oxide for hydrogen evolution by water splitting. Russ J Phys Chem A 92(5):968–975
12. Yu JG, Qi LF, Jaroniec M (2010) Hydrogen production by photocatalytic water splitting over Pt/TiO_2 nanosheets with exposed (001) facets. J Phys Chem C 114(30):13118–13125
13. Zhou K, Zhu Y, Yang X, Jiang X, Li C (2011) Preparation of graphene-TiO_2 composites with enhanced photocatalytic activity. New J Chem 35(2):353–359
14. Zhang XF, Zhang BY, Zuo ZX, Wang MK, Shen Y (2015) N/Si co-doped oriented single crystalline rutile TiO_2 nanorods for photoelectrochemical water splitting. J Mater Chem A 3(18):10020–10025
15. Gerbec JA, Magana D, Washington A, Strouse GF (2005) Microwave-enhanced reaction rates for nanoparticle synthesis. J Am Chem Soc 127(45):15791–15800
16. Hu T, Dai K, Zhang J, Zhu G, Liang C (2019) Noble-metal-free Ni_2P as cocatalyst decorated rapid microwave solvothermal synthesis of inorganic–organic CdS-DETA hybrids for enhanced photocatalytic hydrogen evolution. Appl Surf Sci 481:1385–1393
17. Soman B, Challagulla S, Payra S, Dinda S, Roy S (2018) Surface morphology and active sites of TiO_2 for photoassisted catalysis. Res Chem Intermed 44(4):2261–2273
18. Li X, Wang L, Lu X (2010) Preparation of silver-modified TiO_2 via microwave-assisted method and its photocatalytic activity for toluene degradation. J Hazard Mater 177(1):639–647
19. Suwarnkar MB, Dhabbe RS, Kadam AN, Garadkar KM (2013) Enhanced photocatalytic activity of Ag doped TiO_2 nanoparticles synthesized by a microwave assisted method. Ceram Int 40(4):5489–5496
20. Pan LK, Liu XJ, Sun Z, Sun CQ (2013) Nanophotocatalysts via microwave-assisted solution-phase synthesis for efficient photocatalysis. J Mater Chem A 1(29):8299–8326
21. Mendiola-Alvarez SY, Hernandez-Ramirez A, Guzman-Mar JL, Maya-Trevino ML, Caballero-Quintero A, Hinojosa-Reyes L (2019) A novel P-doped Fe_2O_3–TiO_2 mixed oxide: synthesis, characterization and photocatalytic activity under visible radiation. Catal Today 328:91–98
22. Kato K, Xin Y, Shirai T (2019) Structural-controlled synthesis of highly efficient visible light TiO_2 photocatalyst via one-step single-mode microwave assisted reaction. Sci Rep 9(1):4900
23. Liu DY, Wu BH, Mubeen S, Ding KL, Zeng H, Chuong TT, Moskovits M, Stucky GD (2018) Microwave-assisted synthesis of ultrastable Cu@TiO_2 core–shell nanowires with tunable diameters via a redox-hydrolysis synergetic process. ChemNanoMat 4(9):914–918
24. Cheng QF, Deng XY, Zhang HX, Guo RN, Cui YQ, Ma QL, Zhang XY, Cheng XW, Xie MZ, Li B (2018) Microwave assisted construction of Ag–AgBr/reduced TiO_2 nano-tube arrays photoelectrode and its enhanced visible light photocatalytic performance for degradation of 4-chlorphenol. Sep Purif Technol 193:255–263
25. Anwar A, Akbar S, Kazmi M, Sadiqa A, Gilani SR (2018) Novel synthesis and antimicrobial studies of nanoscale titania particles. Ceram Int 44(17):21170–21175
26. Xiao S, Zhang D, Pan D, Zhu W, Liu P, Cai Y, Li G, Li H (2019) A chloroplast structured photocatalyst enabled by microwave synthesis. Nat Commun 10(1):1570
27. Dabodiya TS, Selvarasu P, Murugan AV (2019) Tetragonal to monoclinic crystalline phases change of $BiVO_4$ via microwave-hydrothermal reaction: in correlation with visible-light-driven photocatalytic performance. Inorg Chem 58(8):5096–5110
28. Li H, Xiao SN, Zhou JC, Zhao JJ, Liu FF, Li GS, Zhang DQ (2019) A flexible CdS nanorods-carbon nanotubes/stainless steel mesh photoanode for boosted photoelectrocatalytic hydrogen evolution. Chem Commun 55(19):2741–2744
29. Feng J, Sun Y, Mu J, Chen L, Han T, Miao H, Liu E, Fan J, Hu X (2019) Microwave-assistant synthesis of Au/SnS_2 nanoflowers as improved visible-light responsive photocatalysts. Mater Lett 236:534–537
30. Gusmao SBS, Ghosh A, Marques TMF, Ferreira OP, Lobo AO, Osajima JAO, Luz-Lima C, Sousa RRM, Matos JME, Viana BC (2019) One-pot synthesis of titanate nanotubes decorated with anatase nanoparticles using a microwave-assisted hydrothermal reaction. J Nanomater. https://doi.org/10.1155/2019/4825432
31. Solcova O, Balkan T, Guler Z, Morozova M, Dytrych P, Sarac AS (2014) New preparation route of TiO_2 nanofibers by electrospinning: spectroscopic and thermal characterizations. Sci Adv Mater 6(12):2618–2624
32. Van Hoa N, Ren Y, Shim J-J (2012) Microwave-assisted synthesis of carbon nanotube-TiO_2 nanocomposites in ionic liquid for the photocatalytic degradation of methylene blue. Synth React Inorg Met Org Nano-Met Chem 42(2):296–301
33. Truong QD, Dien LX, Vo DVN, Lee TS (2017) Controlled synthesis of titania using water-soluble titanium complexes: a review. J Solid State Chem 251:143–163
34. Kobayashi M (2016) Synthesis and development of titania with controlled structures. J Ceram Soc Jpn 124(9):863–869
35. Okunaka S, Tokudome H, Abe R (2015) Facile water-based preparation of Rh-doped $SrTiO_3$ nanoparticles for efficient photocatalytic H_2 evolution under visible light irradiation. J Mater Chem A 3(28):14794–14800
36. Haider Z, Kang YS (2014) Facile preparation of hierarchical TiO_2 nano structures: growth mechanism and enhanced photocatalytic H_2 production from water splitting using methanol as a sacrificial reagent. ACS Appl Mater Interfaces 6(13):10342–10352
37. Yoshizawa M, Kobayashi M, Petrykin V, Kato H, Kakihana M (2014) Insights into a selective synthesis of anatase, rutile, and brookite-type titanium dioxides by a hydrothermal treatment of titanium complexes. J Mater Res 29(1):90–97
38. Gutierrez-Tauste D, Zumeta I, Vigil E, Hernandez-Fenollosa MA, Domenech X, Ayllon JA (2005) New low-temperature preparation method of the TiO_2 porous photoelectrode for dye-sensitized solar cells using UV irradiation. J Photochem Photobiol A 175(2–3):165–171

39. Kim JH, Fujita S, Shiratori S (2006) Fabrication and characterization of TiO_2 thin film prepared by a layer-by-layer self-assembly method. Thin Solid Films 499(1–2):83–89
40. Souza VS, Scholten JD, Weibel DE, Eberhardt D, Baptista DL, Teixeira SR, Dupont J (2016) Hybrid tantalum oxide nanoparticles from the hydrolysis of imidazolium tantalate ionic liquids: efficient catalysts for hydrogen generation from ethanol/water solutions. J Mater Chem A 4(19):7469–7475
41. Languer MP, Scheffer FR, Feil AF, Baptista DL, Migowski P, Machado GJ, de Moraes DP, Dupont J, SrR T, Weibel DE (2013) Photo-induced reforming of alcohols with improved hydrogen apparent quantum yield on TiO_2 nanotubes loaded with ultrasmall Pt nanoparticles. Int J Hydrog Energy 38(34):14440–14450
42. Dal'Acqua N, Scheffer FR, Boniatti R, da Silva BVM, de Melo JV, da Silva CJ, Giovanela M, Pereira MB, Weibel DE, Machado G (2013) Photocatalytic nanostructured self-assembled poly(allylamine hydrochloride)/poly(acrylic acid) polyelectrolyte films containing titanium dioxide-gold nanoparticles for hydrogen generation. J Phys Chem C 117(44):23235–23243
43. Backes CW, Scheffer FR, Pereira MB, Teixeira SR, Weibel DE (2014) Photosensitised degradation of organic dyes by visible light using riboflavin adsorbed on the surface of TiO_2 nanotubes. J Braz Chem Soc 25(12):2417–2424. https://doi.org/10.5935/0103-5053.20140268
44. Tsai C-C, Teng H (2006) Structural features of nanotubes synthesized from NaOH treatment on TiO_2 with different post-treatments. Chem Mater 18(2):367–373
45. Alkaim AF, Kandiel TA, Hussein FH, Dillert R, Bahnemann DW (2013) Solvent-free hydrothermal synthesis of anatase TiO_2 nanoparticles with enhanced photocatalytic hydrogen production activity. Appl Catal A Gen 466:32–37
46. Komarneni S, Li D, Newalkar B, Katsuki H, Bhalla AS (2002) Microwave-polyol process for Pt and Ag nanoparticles. Langmuir 18(15):5959–5962
47. Murphy AB (2007) Band-gap determination from diffuse reflectance measurements of semiconductor films, and application to photoelectrochemical water-splitting. Sol Energy Mater Sol Cells 91(14):1326–1337
48. Fan X, Fan J, Hu XY, Liu EZ, Kang LM, Tang CN, Ma YN, Wu HT, Li YY (2014) Preparation and characterization of Ag deposited and Fe doped TiO_2 nanotube arrays for photocatalytic hydrogen production by water splitting. Ceram Int 40(10):15907–15917
49. Pulido Melián E, González Díaz O, Doña Rodríguez JM, Colón G, Navío JA, Macías M, Pérez Peña J (2012) Effect of deposition of silver on structural characteristics and photoactivity of TiO_2-based photocatalysts. Appl Catal B-Environ 127:112–120
50. Moulder JF (1992) Handbook of X-ray photoelectron spectroscopy: a reference book of standard spectra for identification and interpretation of XPS data. Physical Electronics Division, Perkin-Elmer Corporation, Eden Prairie
51. Ferreira OP, Souza AG, Mendes J, Alves OL (2006) Unveiling the structure and composition of titanium oxide nanotubes through ion exchange chemical reactions and thermal decomposition processes. J Braz Chem Soc 17(2):393–402
52. Amarjargal A, Tijing LD, Kim CS (2012) Effect of annealing on the phase transition and morphology of Ag NPs on/in TiO_2 rods synthesized by a polyol method. Ceram Int 38(8):6365–6375
53. Li H, Duan X, Liu G, Liu X (2008) Photochemical synthesis and characterization of Ag/TiO_2 nanotube composites. J Membr Sci 43(5):1669–1676. https://doi.org/10.1007/s10853-007-2387-y
54. Wodka D, Bielaska E, Socha RP, Elsebieciak-Wodka M, Gurgul J, Nowak P, Warszynski P, Kumakiri I (2010) Photocatalytic activity of titanium dioxide modified by silver nanoparticles. ACS Appl Mater Interfaces 2(7):1945–1953
55. Ajmal A, Majeed I, Malik RN, Idriss H, Nadeem MA (2014) Principles and mechanisms of photocatalytic dye degradation on TiO_2 based photocatalysts: a comparative overview. RSC Adv 4(70):37003–37026
56. Rauf MA, Ashraf SS (2009) Fundamental principles and application of heterogeneous photocatalytic degradation of dyes in solution. Chem Eng J 151(1–3):10–18
57. Herrmann J-M (1999) Heterogeneous photocatalysis: fundamentals and applications to the removal of various types of aqueous pollutants. Catal Today 53(1):115–129
58. Gelderman K, Lee L, Donne SW (2007) Flat-band potential of a semiconductor: using the Mott–Schottky equation. J Chem Educ 84(4):685
59. Baumanis C, Bahnemann DW (2008) TiO_2 thin film electrodes: correlation between photocatalytic activity and electrochemical properties. J Phys Chem C 112(48):19097–19101
60. Liu H, Tian K, Ning J, Zhong Y, Zhang Z, Hu Y (2019) One-step solvothermal formation of Pt nanoparticles decorated Pt^{2+}-doped α-Fe_2O_3 nanoplates with enhanced photocatalytic O_2 evolution. ACS Catal 9(2):1211–1219
61. He B, Liu H, Lin Z, Yan L, Ning J, Zhong Y, Zheng C, Zhang Z, Hu Y (2019) A new photocatalyst based on $Co(CO_3)_{0.5}(OH)\cdot 0.11H_2O$/$Bi_2WO_6$ nanocomposites for high-efficiency cocatalyst-free O_2 evolution. Chem Eng J 359:924–932
62. Sellers MCK, Seebauer EG (2011) Measurement method for carrier concentration in TiO_2 via the Mott–Schottky approach. Thin Solid Films 519(7):2103–2110
63. Premkumar J (2004) Development of super-hydrophilicity on nitrogen-doped TiO_2 thin film surface by photoelectrochemical method under visible light. Chem Mater 16(21):3980–3981
64. Zhang G, Monllor-Satoca D, Choi WY (2013) Band energy levels and compositions of CdS-based solid solution and their relation with photocatalytic activities. Catal Sci Technol 3(7):1790–1797